Supplementary Information: CRI-HOM: A novel chemical mechanism for simulating Highly Oxygenated Organic Molecules (HOMs) in global chemistry-aerosol-climate models.

James Weber[1], Alexander T. Archibald[1,2], Paul Griffiths[1,2], Scott Archer-Nicholls[1], Torsten Berndt[3], Michael Jenkin[4], Hamish Gordon[5], Christoph Knote[6]

[1]Centre for Atmospheric Science, Department of Chemistry, University of Cambridge, Cambridge, CB2 1EW, UK
[2]National Centre for Atmospheric Science, Department of Chemistry, University of Cambridge, CB2 1EW, UK
[3]Atmospheric Chemistry Department (ACD), Leibniz Institute for Tropospheric Research (TROPOS), Leipzig, 04318, Germany
[4]Atmospheric Chemistry Services, Okehampton, Devon, UK
[5]College of Engineering, Carnegie Mellon University, Pittsburgh, PA 15213, USA
[6]Meteorologisches Institut, Ludwig-Maximilians-Universität München, Munich, 80333, Germany

Correspondence to: James Weber (jmw240@cam.ac.uk)

Table S1 - Summary of RO_2-RO_2 rate coefficients

Reaction	Rate Coefficient / cm^3 $molecules^{-1}$ s^{-1}	Reference	Comments
All O3RO2 + $RO2_b$ = 0.5 C20d	**$0.97 - 3.6 \times 10^{-11}$ (See full reaction list)**	**Berndt et al., 2018b**	**Based on Berndt et al, then fitted to data**
All OHRO2 + $RO2_b$ = 0.5 C20d	**$0.4 - 3.5 \times 10^{-11}$ (See full reaction list)**	**Berndt et al., 2018b**	**Based on Berndt et al, then fitted to data**
All O3RO2 + $RO2_b$ = C10x/CARB16	**1.68×10^{-12}**	**Molteni et al., 2019**	
All O3RO2 + $RO2_b$ = Closed shell + peroxy radical	**1.68×10^{-12}**	**Molteni et al., 2019 Jenkin et al., 2019a**	
RN26BO2 + $RO2_m$, $RO2_s$ = C10x/TNCARB26	**8.3×10^{-13}**	**Jenkin et al., 2019a***	**Weighted average of rate coefficients**
RTN28AO2 + $RO2_b$, $RO2_m$, $RO2_s$ = Closed shell	**5.9×10^{-13}**	**MCM**	**Weighted average of RO2 rate coefficients for species APINAO2 and APINBO2**
RTN28BO2 + $RO2_m$, $RO2_s$ = Closed shell + peroxy radical	**6.70×10^{-15}**	**MCM**	**MCM value for species APINCO2**

2nd – 5th gen O3RO2 + $RO2_m$, $RO2_s$ = Closed shell + peroxy radical	**$5 \times 10^{-12} – 1 \times 10^{-11}$ (See full reaction list)**	**Roldin et al., 2019**	**Increases with increasing O3RO2 functionality**
2nd – 5th gen OHRO2 + $RO2_b$, $RO2_m$, $RO2_s$ = Closed shell + peroxy radical	**$5 \times 10^{-12} – 1 \times 10^{-11}$ (See full reaction list)**	**Roldin et al., 2019**	**Increases with increasing OHRO2 functionality**
All O3RO2 + $RO2_m$ = C15d	**$3 - 5\times 10^{-12}$ (See full reaction list)**	**Berndt et al., 2018b**	**Based on Berndt et al, then fitted to data**
All OHRO2 + $RO2_m$ = C15d	**$1.2 - 2.5 \times 10^{-12}$ (See full reaction list)**	**Berndt et al., 2018b**	**Based on Berndt et al, then fitted to data**

* The rate coefficient for the production of the closed shell and alkoxy radical from reaction of the first generation O3RO2 species, RN26BO2, with $RO2_m$ and $RO2_s$ was taken to be the average of the rate coefficients of the three actual species (C107O2, C109O2 and C10BO2 using the notation of Molteni et al (2019)), weighted by the branching ratio of their production. The rate coefficients for C107O2, C109O2 and C10BO2 were calculated using the methodology of Jenkin et al (2019a).

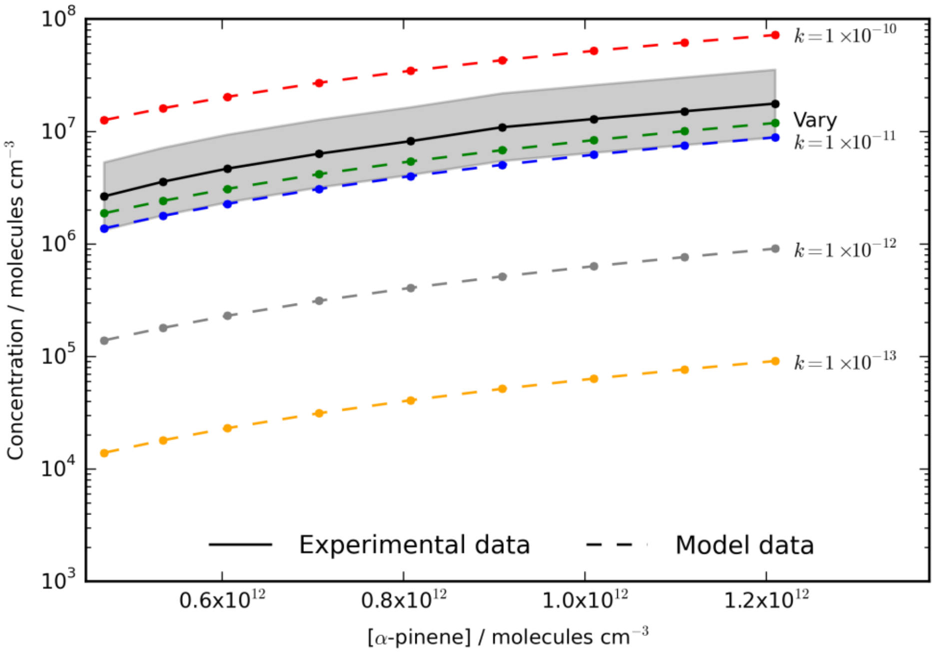

Figure S1 – Effect of C20d formation rate coefficient on model performance compared to observations from Berndt et al (2018b) under varying initial conditions of α-pinene (Simulation A, Table 3). The model was able to reproduce observed concentrations within experimental error (shaded region) here and in Fig 5 when the rate coefficients were increased with increasing peroxy radical functionalisation (line marked “Vary”). The lines with k= 1×10^{-10}, 1×10^{-11}, 1×10^{-12} and 1×10^{-13} show model performance when the specified rate coefficient (in units of cm^3 molecules^{-1} s^{-1}) was used for all O3RO2 and OHRO2. The simulations with accretion formation rate coefficients suggested by Roldin et al (2019) (~ 10^{-13}-10^{-12} cm^3 molecules^{-1} s^{-1}) produced significantly lower C20d concentrations while using rate coefficients suggested by Molteni et al (2019) (≥ 10^{-10} cm^3 molecules^{-1} s^{-1}) overpredicted C20d concentrations.

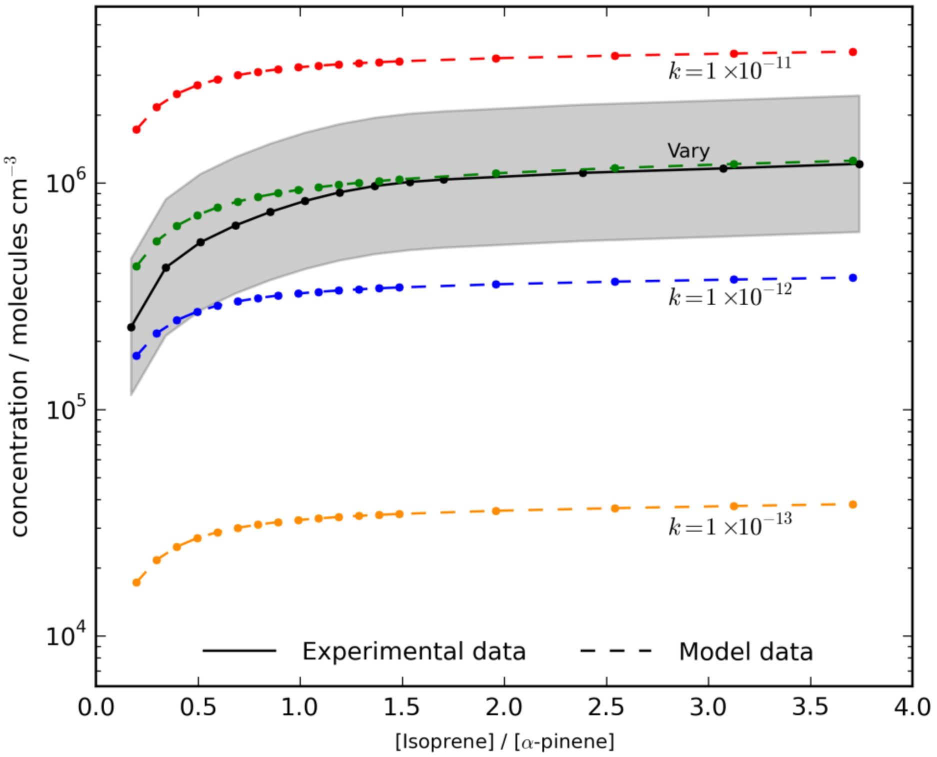

Figure S2 – Effect of C15d formation rate coefficient on model performance compared to observations from Berndt et al (2018b) under conditions of fixed initial α-pinene concentration and varying initial isoprene concentration (Simulation B, Table 3). The model was able to replicate the general trend of increasing C15d with isoprene when the rate coefficients were increased with increasing peroxy radical functionalisation (line marked "Vary"), reproducing observation within experimental error (shaded region). The lines with k=1×10^{-11}, 1×10^{-12} and 1×10^{-13} show model performance when the specified rate coefficient (in units of cm^3 molecules^{-1} s^{-1}) was used for all O3RO2 and OHRO2.

Table S2 - Summary of HOM mechanisms and autoxidation activation energies

Mechanism	Autoxidation Activation Energy / K	Comments
HOM_{TI}	N/A - temperature independent	Autoxidation coefficients based on fitting from data from Berndt et al (2018b) at 297K
HOM_{6000}	6000	Representing possible lower bound of activation energy
HOM_{9000}	9000	Representing possible middle value of activation energy
HOM_{12077}	12077	Value suggested by Roldin et al (2019)

HOM Yield Equations

The yields for 10-carbon HOMs from ozonolysis (γ_{C10z}), OH oxidation (γ_{C10x}) and the total HOM yield (γ_{total}) are given by Eq. 1, Eq. 2 and Eq. 3 respectively.

$$\gamma_{C10x} = \frac{[C10x](k_{OH+HOM}+CS+J)}{k_{OH}[OH][AP]} \quad (1)$$

$$\gamma_{C10z} = \frac{[C10z](k_{OH+HOM}+CS+J)}{k_{O_3}[O_3][AP]} \quad (2)$$

$$\gamma_{total} = \frac{([C10z]+[C10x])(k_{OH+HOM}+CS+J)}{(k_{O_3}[O_3]+k_{OH}[OH])[AP]} \quad (3)$$

where $[O_3]$, $[OH]$, $[C10z]$ and $[C10x]$ are the concentrations of O_3, OH and the 10-carbon HOMs formed from ozonolysis and OH oxidation respectively, k_{OH+HOM} is the rate coefficient for the reactions of HOMs with OH, CS is the HOM condensation sink, J is the HOM photolysis frequency and k_{O_3} and k_{OH} are the reaction rate coefficients of α-pinene with O_3 and OH respectively.

Comparison to CRI v2.2

The new mechanism and the CRI v2.2 were run in a box model (Simulation D, Table 3) for 8 days with varying temperature (298 K average, amplitude of 4 K) and emissions of isoprene and α-pinene varying sinusoidally (Fig S3). Time-independent base NO emissions of $4.7\text{x}10^9$ molecules m^{-2} s^{-1} were used with scaling factors of 1, 3, 10, 30, 100 and 200 employed in a manner consistent with Jenkin et al (2015). Time dependent isoprene emissions reached a maximum of $1.1\text{x}10^{12}$ molecules m^{-2} s^{-1} at 13:00 local time and had an average of $7.1\text{x}10^{11}$ molecules m^{-2} s^{-1} over the period 06:00 to 18:00, similar to emissions used in Jenkin et al (2015) and Bates et al (2019). Time dependent base α-pinene emissions with a mean of $3.23\text{x}10^9$ molecules m^{-2} s^{-1} and maximum of $5.30\text{x}10^9$ molecules m^{-2} s^{-1} at 1500 hours were applied. Further runs were performed with α-pinene emissions scaled by factors of 10^{-3}, 10^{-2}, 0.1, 0.2, 0.5, 1, 2, 3 and 5 to investigate the model's performance. Initial conditions of CH_4 (1.8 ppm), CO (100 ppb), O_3 (20 ppb) and HCHO (300 ppt) were applied.

Photolysis frequencies simulating conditions at the equator also varied in the diurnal cycle. The box model simulated an instantaneously well-mixed planetary boundary with mixing with the free troposphere (with same composition of initial conditions) represented by the box height increasing from 250 m at night to 1500 m at midday before collapsing back to 250 m at 2100 hours.

The "concentration" of a species was taken to be the mean daytime concentration on the 8th day, the metric used by Jenkin et al (2015) and Bates et al (2019). The performance of all the HOM mechanisms (HOM_{TI}, HOM_{6000}, HOM_{9000} and HOM_{12077}) was compared to the CRI v2.2.

The HOM mechanisms matched the CRI extremely well for OH, O_3, NO, NO_2, HO_2, α-pinene and isoprene as well as the hydroperoxides and nitrates derived from isoprene, methyl vinyl ketone and methacrolein, and the important SOA precursor isoprene epoxy diol (IEPOX)).

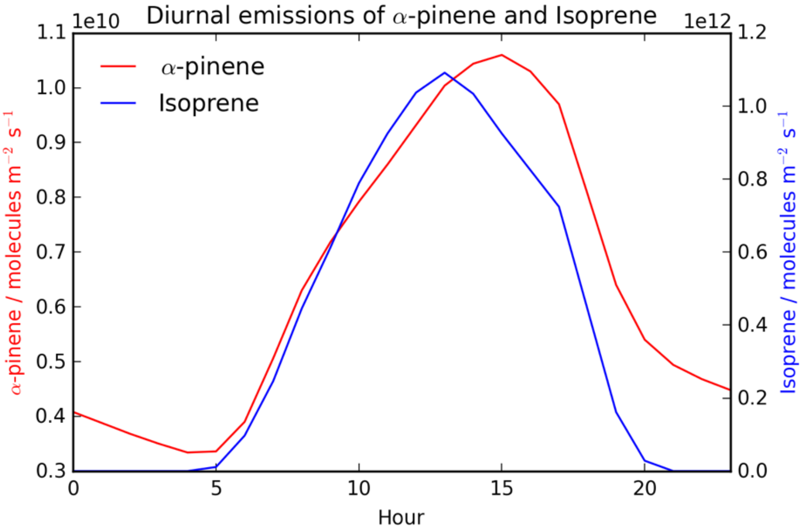

Figure S3 - Diurnal cycle of emissions of α-pinene and isoprene for 8-day comparison of CRI v2.2 R5 with HOM mechanism versions.

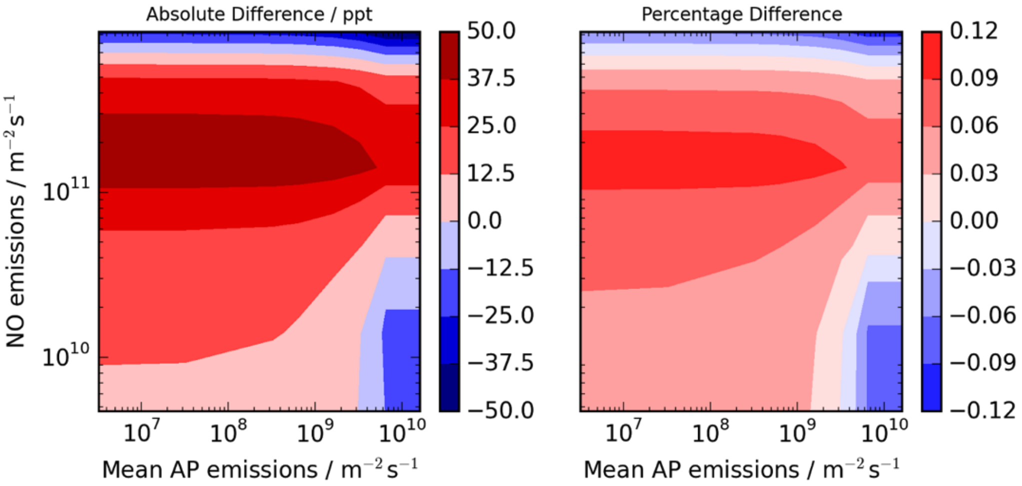

Figure S4 - Absolute and percentage difference in 8th day daylight mean O_3 between the CRI v2.2 R5 and the HOM_{9000} mechanism. The difference between mechanisms is less than ±0.05 ppb.

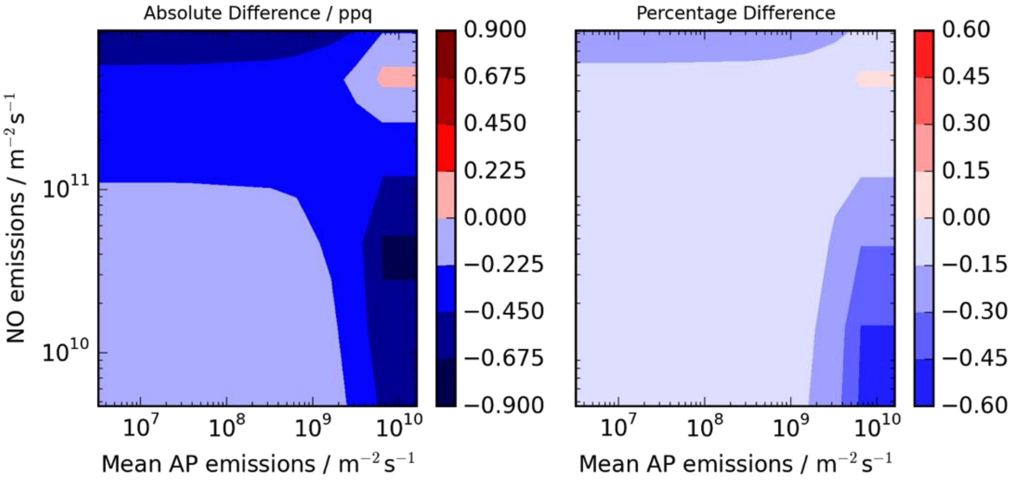

Figure S5 - Absolute and percentage difference in 8th day daylight mean OH between the CRI v2.2 R5 and the HOM_{9000} mechanism. The difference between mechanisms is less than ±0.3% for the vast majority of the emissions space with the difference exceeding this only under very high emissions of α-pinene.

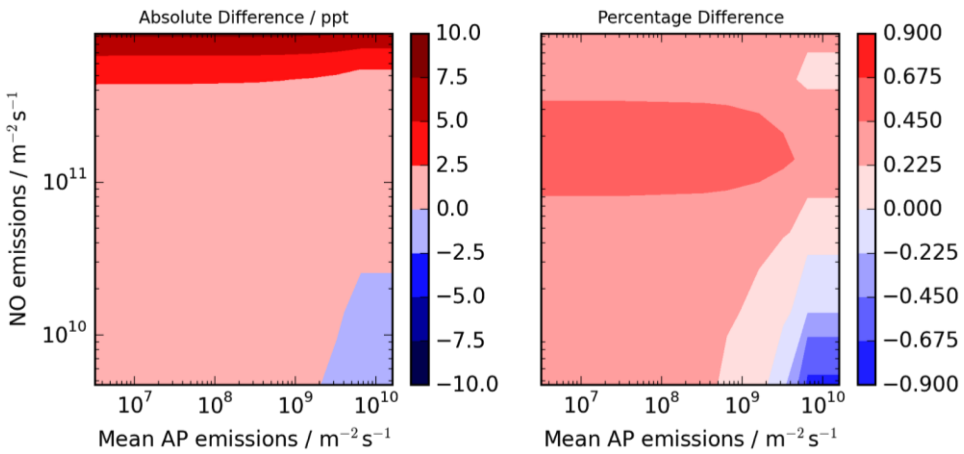

Figure S6 - Absolute difference in 8th day daylight mean NO between the CRI v2.2 R5 and the HOM$_{9000}$ mechanism. The difference between mechanisms is less than ±2.5 ppt for the vast majority of the emissions space with the difference exceeding this only under very high emissions of NO and α-pinene.

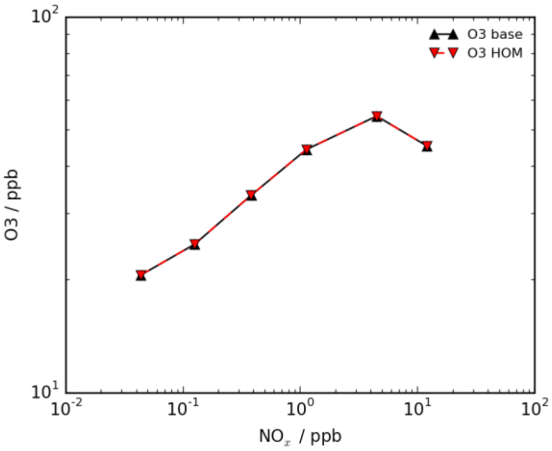

Figure S7 - 8th day daylight mean O$_3$ in CRI v2.2 R5 and HOM$_{9000}$ model

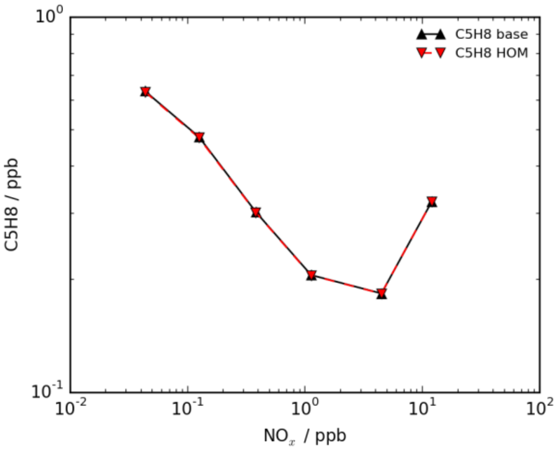

Figure S8 - 8th day daylight mean isoprene in CRI v2.2 R5 and HOM$_{9000}$ model

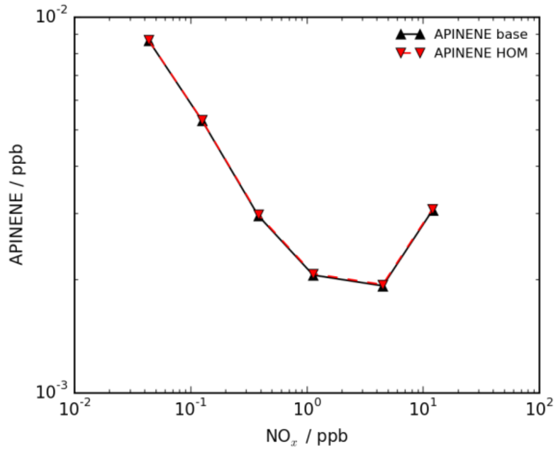

Figure S9 - 8th day daylight mean α-pinene in CRI v2.2 R5 and HOM$_{9000}$ model

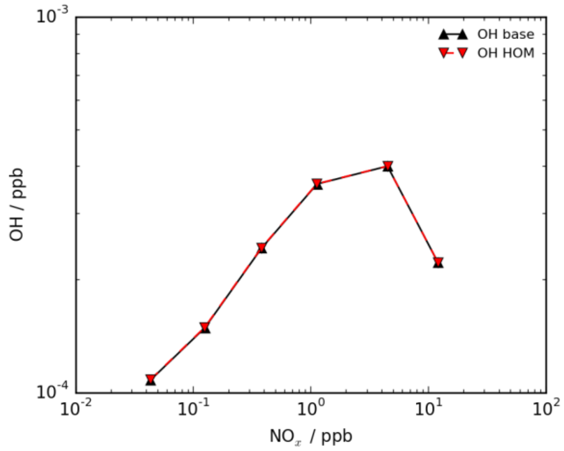

105

Figure S10 - 8th day daylight mean OH in CRI v2.2 R5 and HOM$_{9000}$ model

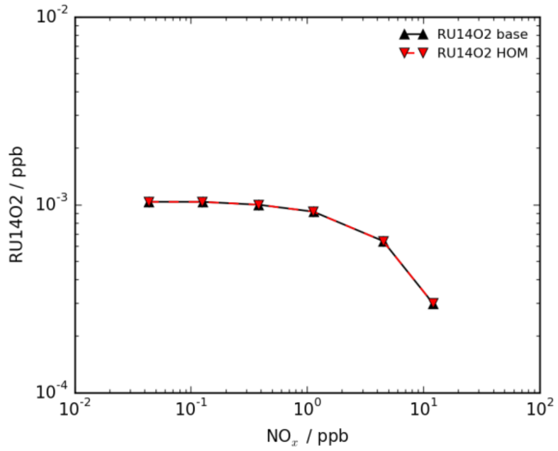

Figure S11 - 8th day daylight mean 1st generation isoprene peroxy radical in CRI v2.2 R5 and HOM$_{9000}$ model

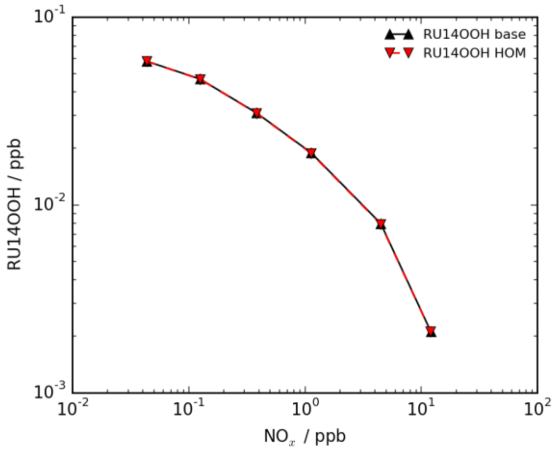

Figure S12 - 8th day daylight mean 1st generation isoprene hydroperoxide in CRI v2.2 R5 and HOM_{9000} model

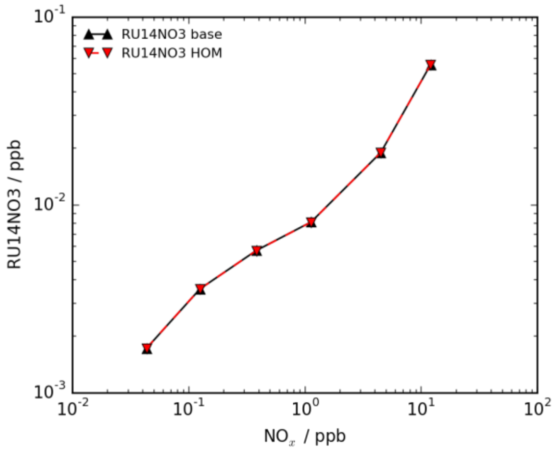

Figure S13 - 8th day daylight mean 1st generation isoprene nitrate in CRI v2.2 R5 and HOM_{9000} model

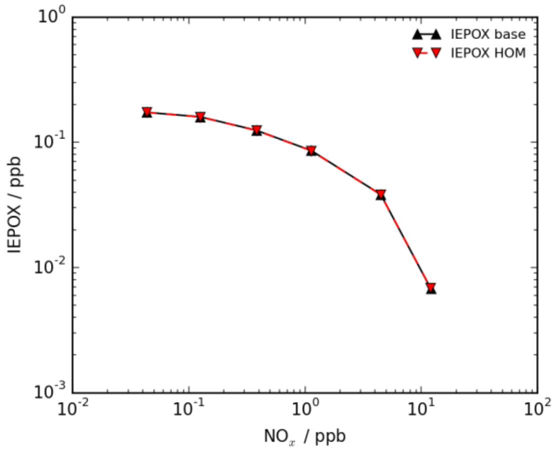

Figure S14 - 8th day daylight mean isoprene epoxydiol in CRI v2.2 R5 and HOM_{9000} model

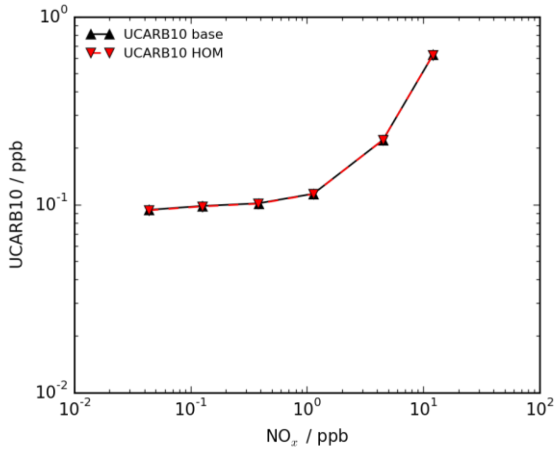

Figure S15 - 8th day daylight mean combined methyl vinyl ketone and methacrolein in CRI v2.2 R5 and HOM$_{9000}$ model

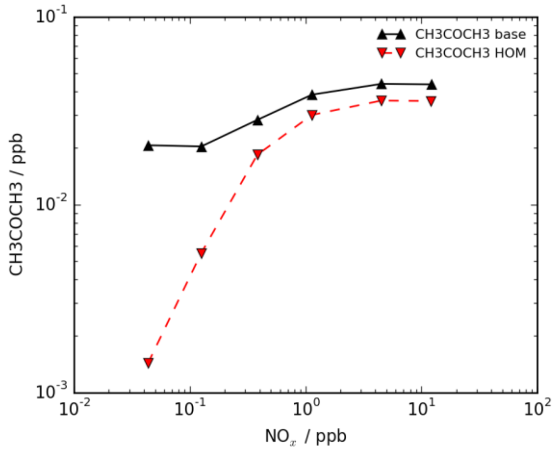

Figure S16 - 8th day daylight mean combined acetone in CRI v2.2 R5 and HOM$_{9000}$ model. The difference was attributed to the added competition supplied by the autoxidation pathways, diverting the degradation of α-pinene away from the traditional pathways which form acetone. However, this discrepancy between mechanisms did not led to significant disagreement between the HOM mechanism and CRI v2.2 R5 for O_3 and OH concentrations.

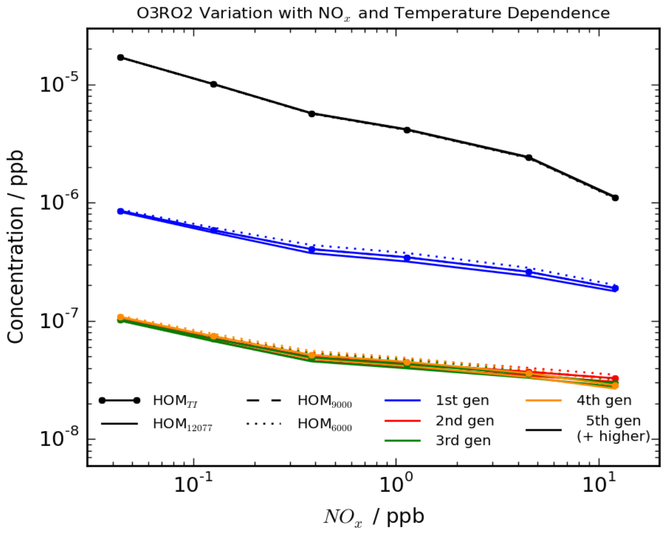

Figure S17 – Peroxy radicals from ozonolysis (O3RO2) exhibiting a decrease with NO_x and the clear dominance of the highest generation peroxy radical. Negligible difference is observed between the 4 HOM mechanisms for each peroxy radical.

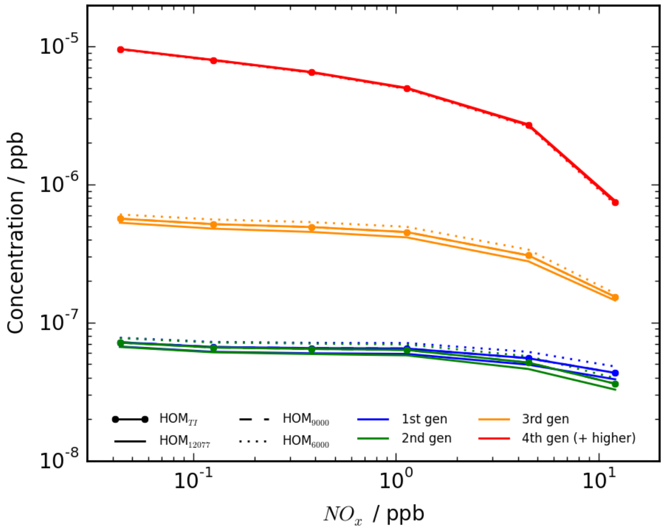

Figure S18 – Peroxy radicals from OH oxidation (OHRO2) exhibiting a decrease with NO_x and the clear dominance of the highest generation peroxy radical. Negligible difference is observed between the 4 HOM mechanisms for each peroxy radical.

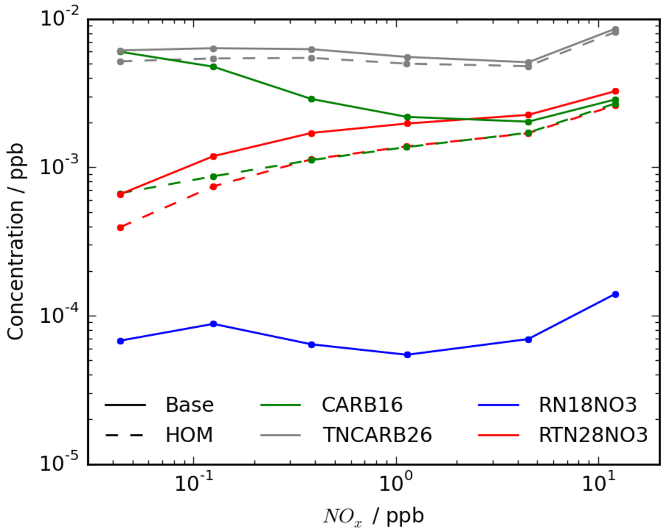

Figure S19 – Closed shell species in base mechanism compared to HOM_{TI} mechanism. The lower concentrations of TNCARB26, CARB16 and RTN28NO3 were attributed to the increased competition from the autoxidation pathways in the HOM mechanism. RN18NO3 was significantly lower in the HOM mechanisms (not shown) as discussed in the main text.

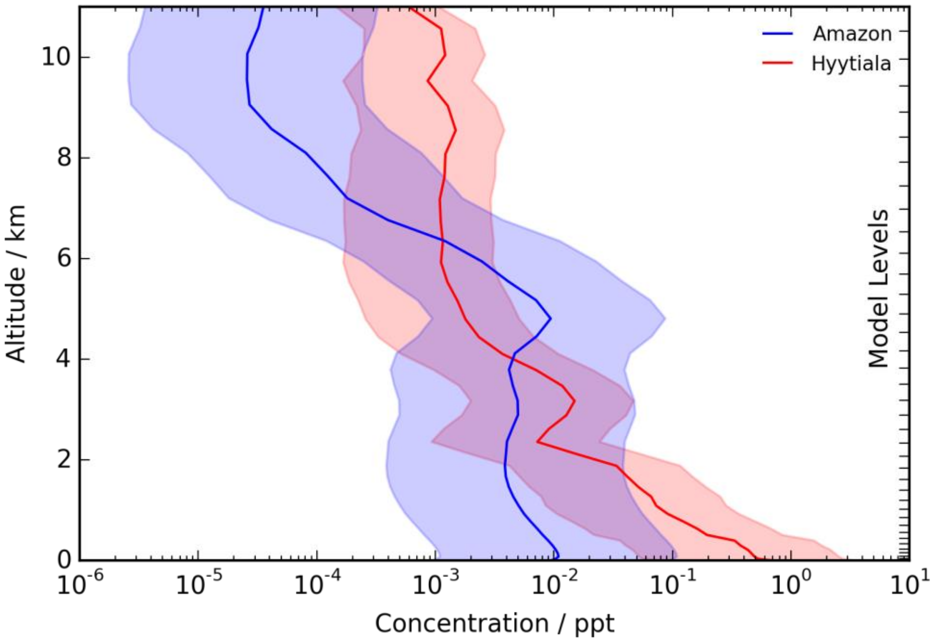

Figure S20 – Total HOM concentrations in Amazon and Hyytiala with shaded region showing the effect of increasing/decreasing CS by a factor of 10. The value of the CS has a significant influence on HOM concentrations.

Table S3 – Species and physical parameters used in the HOM altitude profile modelling. Note that for nucleation calculations, the same input species and parameters were used but all data were monthly means.

Data from UKCA run (2pm 16th June, averaged over 2010-2104)	Data from UKESM Historical
Temperature, pressure, O_3, OH, isoprene, monoterpene*, NO, NO_2, NO_3, N_2O_5, CO, HO_2, H_2O	CH_4, CO, HCHO, CH_3O_2, $C_2H_5O_2$, isoprene nitrate and hydroperoxides, H_2O_2, CH_3OOH, HONO, C_2H_6, C_2H_5OOH, CH_3CHO, PAN, C_3H_8, C_3H_7OOH, C_2H_5CHO, CH_3NO_3, Methacrolein, Methylglyoxal, HCOOH, CH_3CO_3, $C_3H_7O_2$, $C_2H_5CO_3$, CH_3OH

* The modelled monoterpene concentration was halved to approximate the α-pinene concentration (Rinne et al., 2002)

Table S4 - Values of surface level CS and local time of run used for HOM altitude profiles (Lee et al., 2016)

	Location		
	Hyytiala	Manaus	Brent, Alabama
CS / s^{-1}	0.004	0.9	0.012 ± 0.006
Local time	14:00	14:00	12:00

Nucleation Parameterisations

The rates of neutral and ion-induced pure biogenic nucleation (J_n and J_{iin} respectively) are described by the parameterisations (Kirkby et al (2016)) in Eq. 4 and Eq. 5:

$$J_n = a_1[HOM]^{a_2+\frac{a_5}{[HOM]}} \quad (4)$$

$$J_{iin} = a_3[HOM]^{a_4+\frac{a_5}{[HOM]}}[n_{\pm}] \quad (5)$$

Where $a_i$are fitted parameters and $[n_{\pm}]$ the concentration of ions calculated by method described Kirkby et al (2016). In this work, no distinction was made between the different HOM species; the [HOM] term was taken as the sum of all HOM species. In reality, the larger accretion products are likely to be better at nucleating due to their lower volatility and even among 10-carbon HOMs, more oxidised species will also be more proficient at new particle formation. The condensation sink for ions was calculated by summing over aerosol modes and (Eq. 6).

$$CS = \frac{2kT\mu}{\varepsilon}\sum(wd \times c) \times 10^6 \quad (6)$$

Where k is the Boltzmann constant, T temperature (in Kelvin), μ=1.2 x 10^{-4} m^2 V^{-1} s^{-1}, ε =1.6022 x 10^{-19} C, wd is the wet diameter (in m) of the aerosol mode and c the mode's particle concentration (per cm^3) (wd and c were taken from UKCA run).

The ion loss rate, X, was then calculated as the sum of the condensation and nucleation sinks (Eq. 7).

$$X = CS + a_3[HOM]^{a_4+\frac{a_5}{[HOM]}} \quad (7)$$

The recombination coefficient, α, is given by Eq. 8:

$$\alpha = 6 \times 10^{-8}\sqrt{\frac{300}{T}} + 6 \times 10^{-26}c_{air}\left(\frac{300}{T}\right)^4 \quad (8)$$

Where c_{air} is the concentration of air in molecules per cm^3.

$$[n_{\pm}] = \frac{\sqrt{(X^2-4\alpha q)}-X}{2\alpha} \quad (9)$$

Where q is the rate of ion-pair production in cm^{-3} s^{-1}.

The sulphuric acid activation parameterisation used was that developed by Kulmala et al (2006) with coefficient from Sihto et al (2006) as used by Scott et al (2014) (Eq. 10).

$$J_{act} = A[H_2SO_4]$$

(10)

Where A=2x10^{-6} s^{-1}

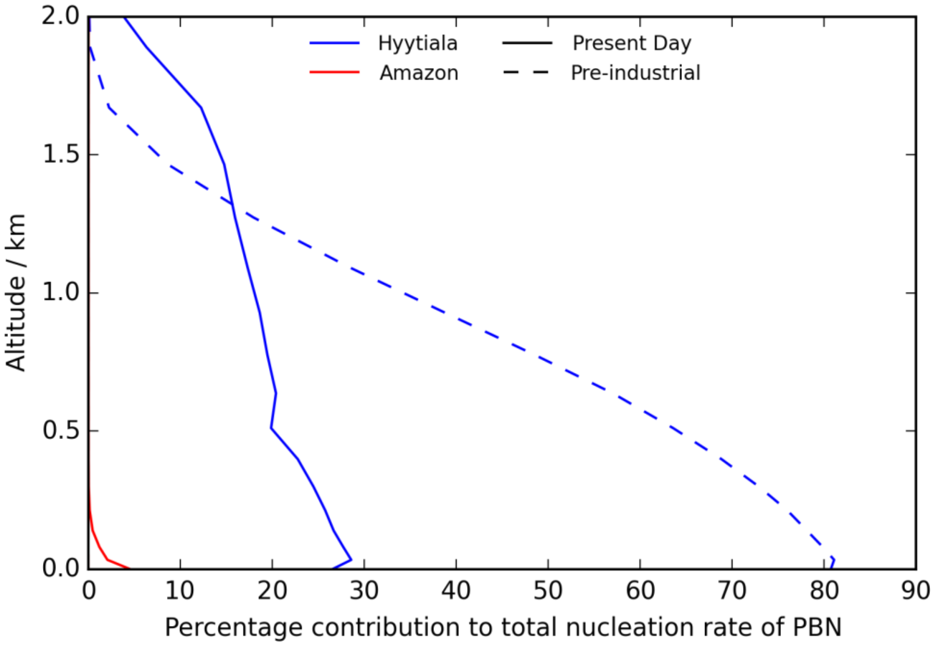

Figure S21 – Percentage contribution to total nucleation rate (PBN + SA_{act}) of PBN. Significant increase is predicted for the PI Hyytiala case in particular, indicating the important implications of including PBN in climate models.

Changes to CRI v2.2 R5 mechanism

Simple rate coefficients (e.g. kRO2NO) and photolysis frequencies (e.g. J41) were taken from CRI (Jenkin et al., 2008, Jenkin et al., 2019b). Unless otherwise stated, unimolecular rate coefficients have units of s^{-1}. The peroxy radical pools ($RO2_b$, $RO2_m$, $RO2_s$ and RO2) represent the total concentration of peroxy radicals falling within the respective pool. In the mechanism used in modelling, certain reactions were lumped together with product fractions weighted by relative rate coefficients to reduce the total number of reactions. For clarity, reactions have been decomposed below. The autoxidation coefficients provided are those fitted at 297 K. Table S5 shows the expressions for the autoxidation coefficients in the 3 temperature dependent mechanisms.

The standard reactions rate coefficients used by the CRI are as follows:

KRO2NO = 2.7D-12*EXP(390/TEMP)

KRO2HO2 = 2.91D-13*EXP(1300/TEMP)

KRO2NO3 = 2.3D-12

Reactions removed from CRI v2.2 R5 mechanism

Ozonolysis of alpha pinene and treatment of resulting peroxy radical RN18AO2

APINENE + O3=OH+CH3COCH3+RN18AO2 : 8.05D-16*EXP(-640/TEMP)*0.80 ;

APINENE + O3 = TNCARB26 + H2O2 : 8.05D-16*EXP(-640/TEMP)*0.175 ;

APINENE + O3 = RCOOH25 : 8.05D-16*EXP(-640/TEMP)*0.025 ;

RN18AO2 + NO = CARB16 + HO2 + NO2 : KRO2NO*0.946 ;

RN18AO2 + NO = RN18NO3 : KRO2NO*0.054 ;

RN18AO2 + NO3 = CARB16 + HO2 + NO2 : KRO2NO3 ;

RN18AO2 + HO2 = RN18OOH : KRO2HO2*0.770 ;

RN18AO2 = CARB16 + HO2 : 8.80D-13*RO2 ;

OH oxidation of alpha pinene and treatment of resulting peroxy radical RTN28O2

APINENE + OH = RTN28O2 : 1.20D-11*EXP(444/TEMP) ;

RTN28O2 + NO = TNCARB26 + HO2 + NO2 : KRO2NO*0.767*0.915 ;

RTN28O2 + NO = CH3COCH3 + RN19O2 + NO2 : KRO2NO*0.767*0.085 ;

RTN28O2 + NO = RTN28NO3 : KRO2NO*0.233 ;

RTN28O2 + NO3 = TNCARB26 + HO2 + NO2 : KRO2NO3 ;

RTN28O2 + HO2 = RTN28OOH : KRO2HO2*0.914 ;

RTN28O2 = TNCARB26 + HO2 : 2.85D-13*RO2 ;

Reactions added

Ozonolysis of α-pinene producing 1st generation O3RO2, RN26BO2 - branching ratio set to 50% based on experimental observations of Berndt et al (2018b)

1. APINENE + O3 = 0.4375TNCARB26 + 0.0625RCOOH25 + 0.5OH + 0.5RN26BO2 : 8.05E-16*EXP(-640/TEMP);

Reactions of RN26BO2

Reaction with HO2 forms hydroperoxide species already in CRI, not a HOM due to insufficient oxygens.

2. RN26BO2 + HO2 = RTN26OOH : KRO2HO2*0.9;

Reaction with NO, NO_3 forms next generation O3RO2 via alkoxy radical isomerisation and fragmentation products (smaller RO2, RN9O2, and closed shell species, CARB16) at 50:50 branching ratio). NO also forms small yield of RN18NO3, estimated from original CRI v2.2 R5.

3. RN26BO2 + NO = 0.025RTN28NO3 + 0.487RN25BO2O2 + 0.487CARB16 + 0.487RN9O2 + 0.975NO2: KRO2NO;

4. RN26BO2 + NO3 = 0.5RN25BO2O2 + 0.5CARB16 + 0.5RN9O2 + NO2 : KRO2NO3 ;

Autoxidation of RN26BO2 to 2nd generation O3RO2, RN25BO2O2

5. RN26BO2 = RN25BO2O2 : 0.206 ;

Reactions of RN25BO2O2

Reaction with HO2 forms HOM monomer C10z as product has sufficient oxygens. Reaction with NO, NO_3 follows the same principle as RN26BO2.

6. RN25BO2O2 + HO2 = C10z : KRO2HO2*0.914;

7. RN25BO2O2 + NO = 0.5RN24BO4O2+ 0.5CARB16 + 0.5RN8O2 + NO2: KRO2NO

8. RN25BO2O2 + NO3 = 0.5RN24BO4O2+ 0.5CARB16 + 0.5RN8O2 + NO2 : KRO2NO3 ;

Autoxidation of RN25BO2O2 to 3rd generation O3RO2, RN24BO4O2

9. RN25BO2O2 = RN24BO4O2 : 1.7;

Reactions of RN24BO4O2

10. RN24BO4O2 + HO2 = C10z : KRO2HO2*0.914;

11. RN24BO4O2 + NO = 0.5RN23BO6O2+ 0.5CARB16 + 0.5RN8O2 + NO2: KRO2NO

12. RN24BO4O2 + NO3 = 0.5RN23BO6O2+ 0.5CARB16 + 0.5RN8O2 + NO2 : KRO2NO3 ;

Autoxidation of RN24BO4O2 to 4th generation O3RO2, RN23BO6O2

13. RN24BO4O2 = RN23BO6O2 : 1.7 ;

Reactions of RN23BO6O2

14. RN23BO6O2 + HO2 = C10z : KRO2HO2*0.914;

15. RN23BO6O2 + NO = 0.5RNxBOyO2 + 0.5CARB16 +0.5RN8O2 + NO2: KRO2NO ;

16. RN23BO6O2 + NO3 = 0.5RNxBOyO2 + 0.5CARB16 +0.5RN8O2 + NO2: KRO2NO3 ;

Autoxidation of RN23BO6O2 to lumped "5th generation and higher" O3RO2, RNxBOyO2

17. RN23BO6O2 = RNxBOyO2 : 1.6;

Reactions of RNxBOyO2 - no further autoxidation

18. RNxBOyO2 + HO2 = C10z : KRO2HO2*0.914;

19. RNxBOyO2 + NO = 0.5RNxBOyO2 + 0.5CARB16 + 0.5RN8O2 + NO2: KRO2NO ;

20. RNxBOyO2 + NO3 = 0.5RNxBOyO2 + 0.5CARB16 + 0.5RN8O2 + NO2: KRO2NO3 ;

Reactions of O3RO2 with big peroxy radical pool (RO2_b)

All reactions with $RO2_b$ produce a 20-carbon accretion product at a rate coefficient from fitting to experimental data (Berndt et al., 2018b). Reactions also produce, with equal rate coefficients (from Molteni et al., 2019), closed shell species which are classified as HOMs for all cases (except for the reaction of RN26BO2 which is not sufficiently oxidised) and alkoxy radicals which go on to react as previously described in this work.

21. RN26BO2 = 0.5 C20d : 0.97E-11 $RO2_b$;

22. RN26BO2 = TNCARB26 + 0.5 CARB16 + 0.5 RN25BO2O2 : 1.68E-12 $RO2_b$;

23. RN25BO2O2 = 0.5 C20d : 2.5E-11 $RO2_b$;

24. RN25BO2O2 = C10z + 0.5 RN24BO4O2 + 0.5 CARB16 + 0.5 RN8O2 : 1.68E-12 $RO2_b$;

25. RN24BO4O2 = 0.5 C20d : 3.4E-11 $RO2_b$;

26. RN24BO4O2 = C10z + 0.5 RN23BO6O2 + 0.5 CARB16 + 0.5 RN8O2 : 1.68E-12 $RO2_b$;

27. RN23BO6O2 = 0.5 C20d : 3.6E-11 $RO2_b$;

28. RN23BO6O2 = C10z + 0.5 RNxBOyO2 + 0.5 CARB16 + 0.5 RN8O2 : 1.68E-12 $RO2_b$;

29. RNxBOyO2= 0.5 C20d : 3.6E-11 $RO2_b$;

30. RNxBOyO2 = C10z + 0.5 RNxBOyO2 + 0.5 CARB16 + 0.5 RN8O2 : 1.68E-12 $RO2_b$;

Reactions of O3RO2 with medium and small peroxy radical pools ($RO2_m$ and $RO2_s$)

Reaction of RN26BO2 is based on corresponding species in MCM.

31. RN26BO2 = 0.5RN25BO2O2 + 0.5CARB16 + 0.5RN9O2 + NO2 : 8.13E-13 ($RO2_s$+$RO2_m$) ;

Rate coefficient and branching ratios of later generation O3RO2 with medium and small peroxy radical pools taken from Roldin et al (2019). The alkoxy radical produced goes on to react as described earlier in this work.

32. RN25BO2O2 = 0.3RN24BO4O2 + 0.3CARB16 + 0.3RN8O2 + 0.4C10z: 5E-12 ($RO2_s$+$RO2_m$) ;

33. RN24BO4O2 = 0.2RN23BO6O2 + 0.2CARB16 + 0.2RN8O2 + 0.6C10z: 7E-12 ($RO2_s$+$RO2_m$);

33. RN23BO6O2 = 0.1RNxBOyO2 +0.1CARB16 +0.1RN8O2 + 0.8C10z : 9E-12 ($RO2_s$+$RO2_m$) ;

34. RNxBOyO2 = 0.1RNxBOyO2+0.1CARB16+0.1RN8O2+0.8C10z : 1E-11 ($RO2_s$+$RO2_m$) ;

Rate coefficient of O3RO2 with isoprene-derived peroxy radical from fitting of model to experimental data (Berndt et al, 2018b).

36. RN26BO2 = C15d : 3E-12 $RO2_m$;

37. RN25BO2O2 = C15d : 4E-12 $RO2_m$;

38. RN24BO4O2 = C15d : 5E-12 $RO2_m$;

39. RN23BO6O2 = C15d : 5E-12 $RO2_m$;

40. RNxBOyO2 = C15d : 5E-12 RO2$_m$;

OH oxidation of alpha pinene producing two OHRO2 - RTN28AO2 + RTN28BO2

41. APINENE + OH = 0.78 RTN28AO2 + 0.22 RTN28BO2: 1.20E-11*EXP(440/TEMP);

Reactions of RTN28AO2 are the same as for RTN28O2 in original CRI v2.2 R5 except for accretion product formation. RTN28AO2 does not undergo autoxidation.

42. RTN28AO2 + NO = 0.23RTN28NO3 + 0.77TNCARB26 + 0.77NO2: 2.7D-12*EXP(360/TEMP)*0.767 ;

43. RTN28AO2 + HO2 = RTN28OOH : 2.91D-13*EXP(1300/TEMP)*0.914 ;

44. RTN28AO2 + NO3 = TNCARB26 + HO2 + NO2 : 2.3D-12 ;

45. RTN28AO2 = TNCARB26: 6.65E-13*RO2 ;

46. RTN28AO2 = 0.5 C20d : 0.4E-11*RO2_b ;

47. RTN28AO2 = C15d : 1.2E-12*RO2_m ;

Reactions of RTN28BO2

Reaction with HO2 forms hydroperoxide species already in CRI, not a HOM due to insufficient oxygens.

48. RTN28BO2 + HO2 = RTN28OOH : KRO2HO2*0.914 ;

Reaction with NO, NO$_3$ forms next generation OHRO2 via alkoxy radical isomerisation and fragmentation products (smaller RO2, RN9O2, and closed shell species, CARB16) at 50:50 branching ratio). NO also forms small yield of RN18NO3, estimated from original CRI v2.2 R5.

49. RTN28BO2 + NO = 0.125*RTN28NO3 + 0.875CH3COCH3 + 0.875RN19O2 + 0.875NO2: KRO2NO ;

50. RTN28BO2 + NO3 = CH3COCH3 + RN17O2 + NO2 : KRO2NO3 ;

Autoxidation of RTN28BO2 to produce 2nd generation OHRO2, RTN27BO2O2

51. RTN28BO2 = RTN27BO2O2 : 2.1 ;

Reactions of RTN27BO2O2

Reaction with HO2 forms hydroperoxide species already in CRI, not a HOM due to insufficient oxygens.

52. RTN27BO2O2 + HO2 = RTN28OOH : KRO2HO2*0.914 ;

53. RTN27BO2O2 + NO = 0.5RTN26BO4O2+0.5CARB16 + 0.5RN9O2 +NO2: KRO2NO ;

54. RTN27BO2O2 + NO3 = 0.5RTN26BO4O2+0.5CARB16 + 0.5RN9O2 +NO2: KRO2NO3 ;

Autoxidation of RTN27BO2O2 to produce 3rd generation OHRO2, RTN26BO4O2

55. RTN27BO2O2 = RTN26BO4O2 : 2.1 ;

Reactions of RTN26BO4O2

Hydroperoxide from RTN26BO4O2 has sufficient oxygens to be classified as a HOM.

56. RTN26BO4O2 + HO2 = C10x : KRO2HO2*0.914 ;

57. RTN26BO4O2 + NO = 0.5RTNxBOyO2 + 0.5CARB16 + 0.5RN8O2 +NO2: KRO2NO ;

58. RTN26BO4O2 + NO3 = 0.5RTNxBOyO2+0.5CARB16 + 0.5RN8O2 +NO2: KRO2NO3 ;

Autoxidation of RTN26BO4O2 to produce “4th generation and higher” OHRO2, RTNxBOyO2

59. RTN26BO4O2 = RTNxBOyO2 : 0.25 ;

Reactions of RTNxBOyO2 - no further autoxidation occurs

60. RTNxBOyO2 + HO2 = C10x : KRO2HO2*0.914 ;

61. RTNxBOyO2 + NO = 0.5RTNxBOyO2 + 0.5CARB16 + 0.5RN8O2 +NO2: KRO2NO ;

62. RTNxBOyO2 + NO3 = 0.5RTNxBOyO2 + 0.5CARB16 + 0.5RN8O2 +NO2: KRO2NO3 ;

Reactions of OHRO2 with big peroxy radical pool ($RO2_b$)

Rate coefficient from fitting of model to experimental data (Berndt et al, 2018b).

63. RTN28BO2 = 0.5 C20d : 0.4E-11 $RO2_b$;

64. RTN27BO2O2 = 0.5 C20d : 2.5E-11 $RO2_b$;

65. RTN26BO4O2 = 0.5 C20d : 5.5E-11 $RO2_b$;

66. RTNxBOyO2 = 0.5 C20d : 3.5E-11 $RO2_b$;

Reactions of OHRO2 with medium, small and total peroxy radical pools ($RO2_m$, $RO2_s$ and RO2)

67. RTN28BO2 = 0.7TNCARB26 + 0.3CH3COCH3 + 0.3RN17O2 : 6.7E-15*RO2

68. RTN27BO2O2 = 0.4TNCARB26 + 0.3RTN26BO4O2 + 0.3CARB16 + 0.3RN10O2 : 5E-12*RO2 ;

69. RTN26BO4O2 = 0.4C10x + 0.3RTNxBOyO2 + 0.3CARB16 + 0.3RN9O2: 8E-12*RO2 ;

70. RTNxBOyO2 = 0.8C10x + 0.1RTNxBOyO2 + 0.1CARB16 + 0.1RN8O2 : 1E-11*RO2 ;

Rate coefficient of OHRO2 with isoprene-derived peroxy radical from fitting of model to experimental data (Berndt et al, 2018b).

71. RTN28BO2 = C15d : 1.2E-12 $RO2_m$;

72. RTN27BO2O2 = C15d :2.5E-12 $RO2_m$;

73. RTN26BO4O2 = C15d :2.5E-12 $RO2_m$;

74. RTNxBOyO2 = C15d : 2.5E-12 $RO2_m$;

Photolysis of HOMs

Photolysis of peroxide linkage and carbon linkages were considered using MCM frequencies J41 and J15 respectively. KPP parameter “SUN” was used to experiments were the photolysis frequency was varied.

Photolysis of peroxide linkage in HOM monomer produces one OH and one alkoxy radical which behaves as previously discussed (50% decomposition, 50% isomerisation). As the extent of oxidation of the HOM is unknown, isomerisation produces second generation peroxy radical by default.

75. C10z = 0.5CARB16 + 0.5RN9O2 + 0.5RN25BO2O2 + OH : SUN*J41;

76. C10x = 0.5CARB16 + 0.5RN9O2 + 0.5RTN27BO2O2 + OH: SUN*J41;

Photolysis of C20d produces two alkoxy radicals. The isomerisation products are 2nd gen OHRO2 and 2nd gen O3RO2.

77. C20d = 0.5RN25BO2O2 + 0.5RTN27BO2O2 + RN9O2 + CARB16 : SUN*J41;

Photolysis of C15d produces two alkoxy radicals. The isoprene-derived alkoxy radical produces UCARB12 (as inCRI v2.2 R5) while the alkoxy radical from alpha pinene forms next generation peroxy radicals via isomerisation (50 % OHRO2 and 50% O3RO2) and fragmentation products.

78. C15d = UCARB12 + 0.25RN25BO2O2 + 0.25RTN27BO2O2 + 0.5RN9O2 + 0.5CARB16: SUN*J41;

Photolysis of carbonyl linkage produces an acyl radical and an alkyl radical which will form peroxy radicals. It is assumed that one of these peroxy radical is big enough to be considered (2nd generation) O3RO2 or OHRO2.

79. C10z = RN25BO2O2 : J15;

80. C10x = RTN27BO2O2: J15;

81. C20d = 0.5RN25BO2O2 + 0.5RTN27BO2O2 : J15;

82. C15d = 0.5RN25BO2O2 + 0.5RTN27BO2O2: J15;

HOM loss to OH

All HOM species are lost to OH with same rate coefficient as that for large hydroperoxide RTN28OOH in CRI v2.2 R5. The products, closed shell CRI species CARB10 and CARB15, were chosen under the assumption that the HOM fragments and the sum of CRI indices of the product is close to the CRI index of the peroxy radical which formed the HOM (23-27). The reaction of C15d also produces a product featured in the oxidation pathway of isoprene, UCARB10.

83. C10z + OH = CARB10 + CARB15 + OH : 2.38E-11 ;

84. C10x + OH = CARB10 + CARB15 + OH : 2.38E-11 ;

85. C15d + OH = CARB10 + CARB15 + UCARB10+ OH : 2.38E-11 ;

86. C20d + OH = 2CARB10 + 2CARB15 + OH : 2.38E-11 ;

Table S5 - Temperature dependencies used for 3 temperature dependent mechanism versions.

Species	HOM_{6000}	HOM_{9000}	HOM_{12077}
RN26BO2	1.223E8*EXP(-6000/T)	2.981E12*EXP(-9000/T)	9.413E16*EXP(-12077/T)
RN25BO2O2	1.009E9*EXP(-6000/T)	2.460E13*EXP(-9000/T)	7.768E17*EXP(-12077/T)
RN24BO4O2	1.009E9*EXP(-6000/T)	2.460E13*EXP(-9000/T)	7.768 E17*EXP(-12077/T)
RN23BO6O2	9.500E8*EXP(-6000/T)	2.315E13*EXP(-9000/T)	7.311E17*EXP(-12077/T)
RTN28BO2	1.247E9*EXP(-6000/T)	3.038E13*EXP(-9000/T)	9.595E17*EXP(-12077/T)
RTN27BO2O2	1.247E9*EXP(-6000/T)	3.038E13*EXP(-9000/T)	9.595E17*EXP(-12077/T)
RTN26BO4O2	1.484E8*EXP(-6000/T)	3.617E12*EXP(-9000/T)	1.142E17*EXP(-12077/T)

The uncertainty in the autoxidation coefficients was estimated by further box models simulations where an autoxidation coefficient was adjusted so that the corresponding species was simulated at the upper and lower concentrations values given the experimental uncertainty.

Table S6 - Estimated Uncertainty in Autoxidation Coefficients (at 297 K)

Species	Coefficient / s^{-1}
RN26BO2	0.206 (+0.025/ -0.04)
RN25BO2O2	1.7 (+1.1/-0.4)
RN24BO4O2	1.7(+1.1 / -0.4)
RN23BO6O2	1.6 (+0.8/ -0.5)
RTN28BO2	2.1 Taken directly from Xu et al., 2018
RTN27BO2O2	2.1 (+1.6 / -0.2)
RTN26BO4O2	0.25 (+0.3 /-0.1)

Breakdown of Peroxy Radical Pools In CRI-HOM

Large Peroxy Radical Pool (8 or more carbons)

RTN28AO2, RTN28BO2, RTN27BO2O2, RTN26BO4O2, RTNxBOyO2, RN26BO2, RTN24O2, RN25BO2O2, RN24BO4O2, RN23BO6O2, RNxBOyO2, NRTN28O2, RA19CO2, RTX28O2, NRTX28O2, RTN26O2, RTN25O2, RTX22O2, RTN24O2, RTN23O2

Medium Peroxy Radical Pool (4-7 carbons)

RU12O2, NRU12O2, RN13O2, RN12O2, NRN12O2, RA13O2, DHPR12O2, RN11O2, RA16O2, RU10O2, RU10AO2, MACO3, RN13AO2, RU12O2, NRU12O2, RTN14O2, RN16AO2, RN14O2, RTN10O2, RN17O2, RN15AO2, RN15O2, RN18AO2, RN16O2, RN18O2, RN19O2

Small Peroxy Radical Pool (3 or fewer carbons)

CH3O2, C2H5O2, HOCH2CH2O2, CH3CO3, C2H5CO3, ICH3H7O2, RN10O2, HOCH2CO3, NRN6O2, RN9O2, NRN9O2, RN8O2

Sensitivity Tests

Initial concentrations of 4 ppt of NO, NO_2 and HO_2 ($1x10^8$ cm^{-3}) and $1x10^6$ cm^{-3} OH were used in the modelling of flow cell data from Berndt et al (2018b). The uncertainty in the experimental concentrations of NO, HO_2 and OH has an effect on the modelled concentrations of O3RO2, OHRO2 and accretion products and thus fitted the autoxidation coefficients and accretion production formation rates coefficients. To assess the effect of this uncertainty, multiple model runs were carried out with different initial conditions of NO, HO and HO_2.

NO

NO concentrations were believed to be below $1x10^8$ cm^{-3} (~4 ppt) and initial conditions from $1x10^7$ cm^{-3} (0.4 ppt) to $1x10^{10}$ cm^{-3} (0.4 ppb) were considered with particular attention paid to the range $5x10^7$ - $5x10^8$ cm^{-3}. The O3RO2 exhibited negligible dependence on initial NO while OHRO2 displayed a noticeable but small dependence. Relative to the assumed NO concentration of $1x10^8$ cm^{-3}, NO of $5x10^8$ cm^{-3} increased OHRO2 concentrations by <10% (slightly larger than experimental uncertainty) while NO of $5x10^7$ cm^{-3} led to a decrease of <5%. C20d also exhibited negligible dependence on NO (<2%). Given that NO was likely to be less than $1x10^8$ cm^{-3} and the effect of lowering the concentration further was observed to be considerably smaller than experimental error, the uncertainty in NO was considered of minor importance.

HO_2

The initial concentration HO_2 was varied from $1x10^7$ cm^{-3} (0.4 ppt) to $1x10^{10}$ cm^{-3} (0.4 ppb) (initial NO of $1x10^8$ cm^{-3}). O3RO2 species showed little dependence to initial HO_2 between 0.4 ppt and 80 ppt while OHRO2 exhibited greater dependence with 40 ppt increasing OHRO2 by up to 35% relative to 4 ppt and 0.4 ppt decreasing OHRO2 by < 10% and C20d varied by <±10% from 0.4 ppt to 40 ppt initial HO2 (all within experimental uncertainty).

OH

Initial OH concentration had negligible effect on O3RO2, C20d and OHRO2 even when it was varied over two orders of magnitude ($10^5 – 10^7$ cm^{-3}).

References

Bates, K. H. and Jacob, D. J.: A new model mechanism for atmospheric oxidation of isoprene: global effects on oxidants, nitrogen oxides, organic products, and secondary organic aerosol, Atmos. Chem. Phys., 19, 9613–9640, doi.org/10.5194/acp-19-9613-2019, 2019.

Berndt, T., Mentler, B., Scholz, W., Fischer, L., Herrmann, H., Kulmala, M. and Hansel, A.: Accretion product formation from ozonolysis and OH radical reaction of α-pinene: mechanistic insight and the influence of isoprene and ethylene. Environmental science & technology, 52,11069-11077, doi.org/10.1021/acs.est.8b02210, 2018b.

Jenkin, M. E., Valorso, R., Aumont, B., and Rickard, A. R.: Estimation of rate coefficients and branching ratios for reactions of organic peroxy radicals for use in automated mechanism construction, Atmos. Chem. Phys., 19, 7691–7717, doi.org/10.5194/acp-19-7691-2019, 2019a.

Lee, S.H., Uin, J., Guenther, A.B., de Gouw, J.A., Yu, F., Nadykto, A.B., Herb, J., Ng, N.L., Koss, A., Brune, W.H. and Baumann, K.: Isoprene suppression of new particle formation: Potential mechanisms and implications. Journal of Geophysical Research: Atmospheres, 121,14-621, doi.org/10.1002/2016JD024844, 2016.

Molteni, U., Simon, M., Heinritzi, M., Hoyle, C.R., Bernhammer, A.K., Bianchi, F., Breitenlechner, M., Brilke, S., Dias, A., Duplissy, J. and Frege, C.:. Formation of Highly Oxygenated Organic Molecules from α-Pinene Ozonolysis: Chemical Characteristics, Mechanism, and Kinetic Model Development. ACS Earth and Space Chemistry, 3, 873-883,doi.org/10.1021/acsearthspacechem.9b00035, 2019.

Rinne, H.J.I., Guenther, A.B., Greenberg, J.P. and Harley, P.C.: Isoprene and monoterpene fluxes measured above Amazonian rainforest and their dependence on light and temperature. Atmos Env, 36, 2421-2426. doi.org/10.1016/S1352-2310(01)00523-4, 2002

Roldin, P., Ehn, M., Kurtén, T., Olenius, T., Rissanen, M.P., Sarnela, N., Elm, J., Rantala, P., Hao, L., Hyttinen, N. and Heikkinen, L..: The role of highly oxygenated organic molecules in the Boreal aerosol-cloud-climate system. Nature communications, 10, 1-15, doi.org/10.1038/s41467-019-12338-8, 2019.

Scott, C. E., Rap, A., Spracklen, D. V., Forster, P. M., Carslaw, K. S., Mann, G. W., Pringle, K. J., Kivekäs, N., Kulmala, M., Lihavainen, H., and Tunved, P.: The direct and indirect radiative effects of biogenic secondary organic aerosol, Atmos. Chem. Phys., 14, 447–470, doi.org/10.5194/acp-14-447-2014, 2014.

Sihto, S.-L., Kulmala, M., Kerminen, V.-M., Dal Maso, M., Petäjä, T., Riipinen, I., Korhonen, H., Arnold, F., Janson, R., Boy, M., Laaksonen, A., and Lehtinen, K. E. J.: Atmospheric sulphuric acid and aerosol formation: implications from atmospheric mea- surements for nucleation and early growth mechanisms, Atmos. Chem. Phys., 6, 4079–4091, doi:10.5194/acp-6-4079-2006, 2006

445 Xu, L., Møller, K.H., Crounse, J.D., Otkjær, R.V., Kjaergaard, H.G. and Wennberg, P.O.:. Unimolecular reactions of peroxy radicals formed in the oxidation of α-pinene and β-pinene by hydroxyl radicals. The Journal of Physical Chemistry A, 123, 1661-1674, doi.org/10.1021/acs.jpca.8b11726, 2019.